Supporting Information

Reversible Control of Solubility Using Functionalized Nanoparticles

Authors: Samir A. Kulkarni[1] and Allan S. Myerson[1]*

Affiliations:

[1] Novartis-MIT Center for Continuous Manufacturing and Department of Chemical Engineering, Massachusetts Institute of Technology, 77 Massachusetts Avenue, Cambridge, Massachusetts 02139, United States

*Email to: Myerson@mit.edu.

1. Materials and Methods:

D-Mannitol, benzoic acid, nitrobenzene and sodium chloride with a purity of ≥99%, ≥99%, ≥98% and ≥99%, respectively, were obtained from Sigma Aldrich. DI-water, ethyl acetate and decane were also obtained from Sigma Aldrich. Self-Assembled Gold nanoparticles coated with 2-mercaptoethanol (1.8 and 5.0 nm size) and 1-mercaptodecane (1.8 nm size) was purchased from Nanopartz Inc. Loveland, Colorado.

1.1 Solubility measurements: The solubility and metastable zone width of D-Mannitol was measured in pure DI water and DI water-ethanol mixtures at different concentrations by adding a known amount of D-mannitol and 1 mL of solvent or solvent mixtures respectively to a 1.5 mL glass vial. The Metastable Zone Width (MSZW) is the difference between the saturation temperature and the temperature at which crystals are detected under constant cooling rate. The vials were then placed in the Crystal16 and the heating rate and cooling rate were set to 0.3 °C/min. The samples were stirred with a controlled stirring speed of 700 rpm using magnetic stirring bars. The samples were heated with a heating rate of 0.3 °C/min from 5 °C to 60 °C. The temperature at which the suspension turned into a clear solution was recorded and assumed to be the saturation temperature. After a waiting time of 30 minutes at 60°C the clear solution was cooled to 5 °C with a cooling rate of 0.3 °C/min to recrystallize the mannitol. The temperatures at which the crystals are detected are assumed to be a cloud point. Then the same temperature profile was repeated three times for each sample. A fit of the Van't Hoff equation to the data facilitated the interpolation of the solubility as well as the determination of the prevailing supersaturation ratio $S=x/x^*$ in a certain solution composition.[1]

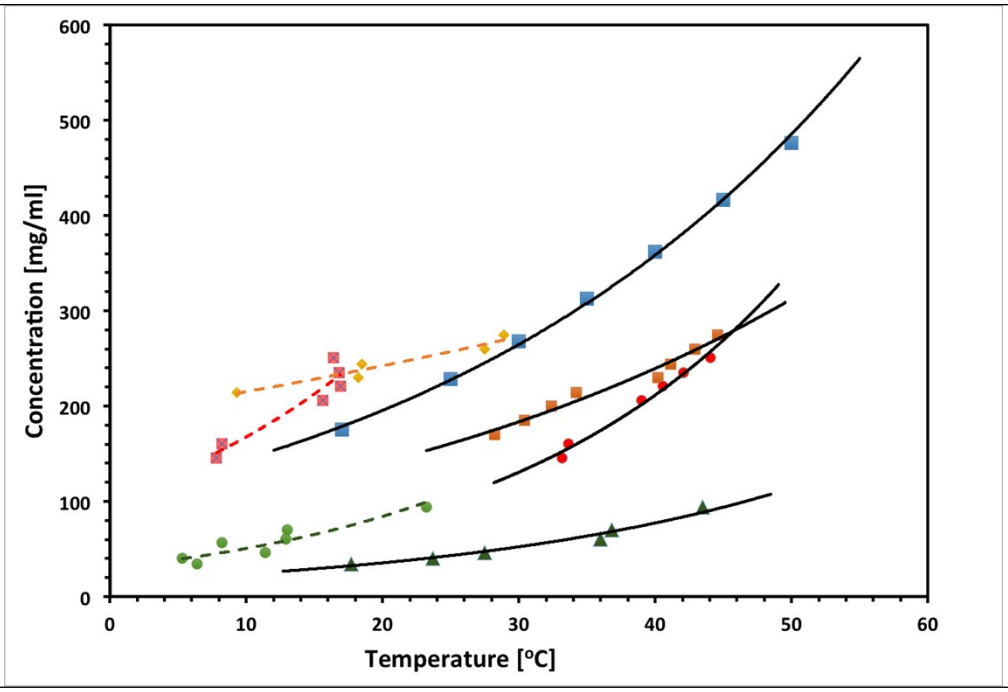

Figure 1: The solubility of D-mannitol in water and water-ethanol mixtures. The line represents the guide to the eye through the saturation temperatures. The cross and circles are the average cloud points were the crystals are detected.

The experimentally determined solubility and the metastable zone width of D-mannitol in water and water-ethanol mixtures (85-15, 75-25 and 50-50 % wt/wt of water-ethanol mixtures) are shown in figure 1. According to the results of D-mannitol in water and water-ethanol mixtures, the solubility decreases with increasing the amount of ethanol in water-ethanol mixtures. In order to know the required amount of functionalized nanoparticles and the operating region for crystallization, the MSZW of D-Mannitol is important. For the samples of D-Mannitol in the mixtures of 85-15 and 75-25 % wt/wt of water-ethanol, the cloud point lies above the saturation temperature of D-mannitol in pure water. Which means that for the mixtures of 85-15 and 75-25 % water ethanol and the solute with concentrations 193 mg/ml at 20 ^{o}C will remain in solution and the spontaneous nucleation will not occur. However these experiments helped to determine the optimum operating supersaturation levels as well as the amount of antisolvent required crystallizing compounds at a given concentration. It also helps to determine if the samples need to be seeded or not. For the solutions of D-mannitol in 50-50% wt/wt water ethanol mixtures the cloud points lies well below the saturation temperature of D-Mannitol in pure water.

The experimentally determined solubility of Fenofibrate in Ethyl acetate and Ethyl acetate-Decane mixtures (95-5% vol/vol) are shown in Figure 2. The solubility of Fenofibrate is lower in ethyl acetate-decane mixture (95-5% vol/vol) as compared to the solubility of fenofibrate in pure ethyl acetate.

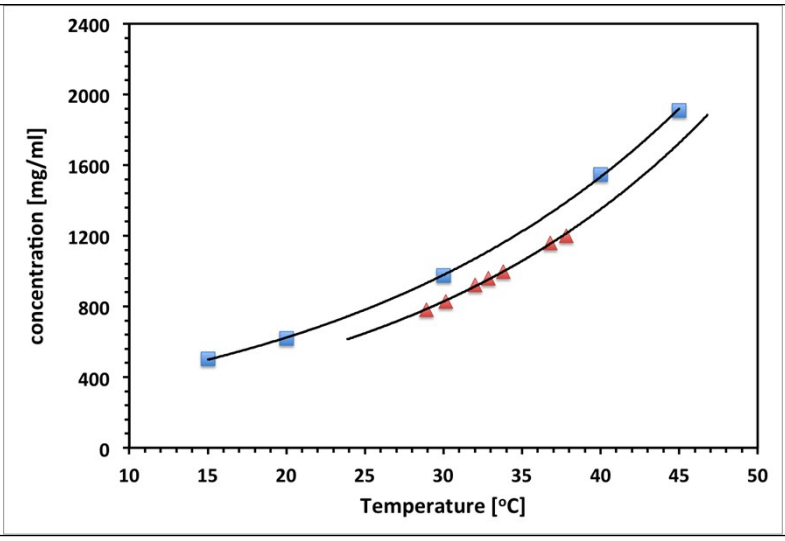

Figure 2: The solubility of Fenofibrate in (a) Ethyl acetate and (b) Ethyl acetate-Decane (95-5% vol/vol) mixtures. The line represents the guide to the eye through the saturation temperatures.

1.2 Preparations of Self-Assembled Monolayers of functionalized gold nanoparticles

Gold nanoparticles (GNP's) functionalized with thiol containing molecules forming self-assembling monolayers are often used as heterogeneous surface to crystallized chemical and pharmaceutical compounds.[2-4] In the present invention, we used functionalized nanoparticles to crystallize organic and inorganic compounds from undersaturated samples similarly as antisolvent crystallization. The knowledge of the surface coverage of functionalized nanoparticles is important to accurately determine the amount of nanoparticles required to replace the volume of antisolvent.

Self-Assembled Gold nanoparticles coated with 2-mercaptoethanol (1.8 and 5.0 nm size) was purchased from Nanopartz Inc. Loveland, Colorado. Iron Oxide Nanoparticles (IONP's) were synthesized by chemical co-precipitation[5, 6] method under alkaline condition and molar ratio between Fe^{2+} salt and Fe^{3+} salt was maintained at 1:2. In order to synthesize 1 g of Fe_3O_4 particle, 0.86 g of $FeCl_2\_4H_2O$ and 2.35 g of $FeCl_3\_6H_2O$ were dissolved in 40 mL ultrapure water under N_2 atmosphere with vigorous stirring at speed of 1000 rpm. As the solution was heated to 80 ^oC, 5 mL of NH_4OH solution was added and the reaction was continued for another 30 min. The resulting suspension was cooled down to room temperature and washed with ultrapure water. The product of bare magnetic nanoparticles (IONP) was isolated from the solvent by magnetic decantation. The IONP's further washed with water 5 times and separation by magnetic decantation. The IONP's are further coated by glycolic acid or decanoic acid by mixing the IONP's with 10M solution of glycolic acid. The mixture was stirred for 24 hours at room temperature and the IONP's are separated by magnetic decantation. The figure 3 shows the (vial 1) hydrophilic nature of IONPs coated with glycolic acid, (vial 2) hydrophobic nature of IONPs coated with decanoic acid in water solutions. Figure 4 shows the TEM images of IONPs coated with glycolic acid. The IONP's are in the range of 5-15 nm in size.

Figure 3: The pictures showing the (vial 1) hydrophilic nature of IONPs coated with glycolic acid in water, (vial 2) hydrophobic nature of IONPs coated with decanoic acid in water solution.

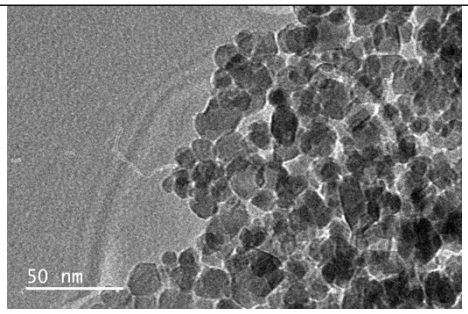

(a)

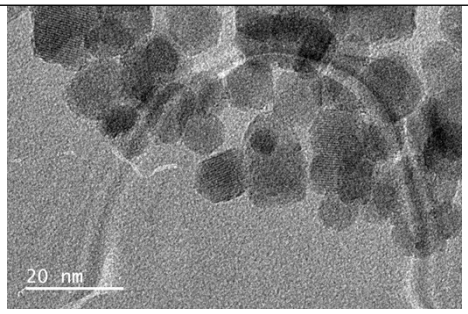

(b)

Figure 4: TEM images of IONPs coated with glycolic acid. Scale bar (a) 50 nm, and (b) 20 nm. The IONP's are in the range of 5-15 nm in size.

The FT-IR spectra of functionalized IONP's

The surface functionalization of the IONPs was analyzed by FT-IR. Figure 5 shows the FT-IR spectrum of the IONP samples. The peaks at around 570 cm^{-1} indicate the presence of iron oxide.[7-9] The peaks at 1700 cm^{-1}, representing the carbonyl stretching vibrations[9], were found shifted in the IONPs at lower wave numbers (1600 cm^{-1}) due to the interaction of IONP surface and carboxylic group of glycolic acid.

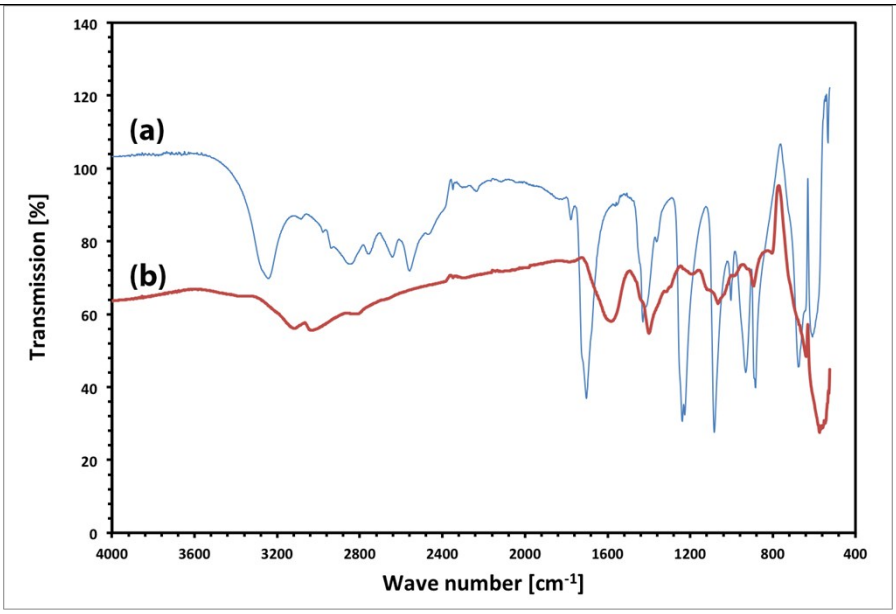

Figure 5: FT-IR spectra of (a) pure glycolic acid and (b) iron oxide nanoparticles with self-assembled monolayers of glycolic acid.

Crystallization using functionalized nanoparticles:

The ESI provides the video of fenofibrate crystallization from ethyl acetate undersaturated solution using decanoic acid coated iron oxide nanoparticles and the dissolution of benzoic acid and 4-nitrophenol from water using iron oxide nanoparticles functionalized with glycolic acid. The more then 2 hours videos were edited in order to attach it to the supplementary information document.

XRPD results:

X-ray powder diffraction data were collected using a PANalytical X'Pert PRO Theta/Theta powder X-ray diffraction system with a Cu tube and X'Celerator high-speed detector. All the XRPD patterns were added as electronic supplementary information (ESI).

A mixture of β-form of D-Mannitol and small traces of gold nanoparticles was the outcome from an XRPD analysis of the powder obtained after filtration (Figure 6). The diffractograms (Figure 10) recorded from the powder XRD of sample show extra peaks at the 2θ position 38.13 (Bragg's plane 111), 44.35 (Bragg's plane 200), 64.73 (Bragg's plane 220) and 77.75 (Bragg's plane 311) indicating a structure of the GNPs.[10]

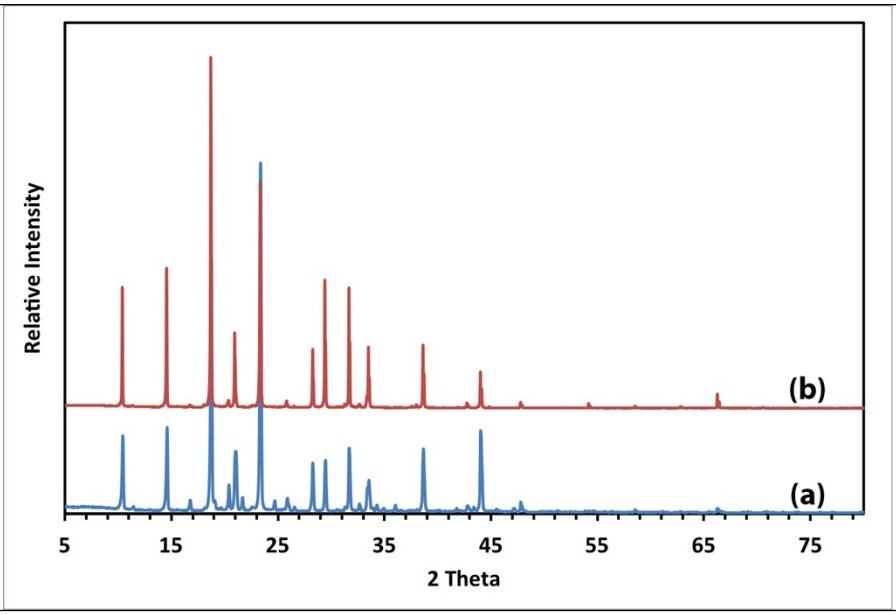

Figure 6: PXRD of solids samples of D-Mannitol, (a) Starting material purchased from Sigma-Aldrich (b) D-Mannitol crystallized from water solution using functionalized gold nanoparticles.

Similar to D-Mannitol the diffractograms (Figure 7) recorded from the powder XRD of sample show extra peaks at the 2θ position 38.13 (Bragg's plane 111), 44.35 (Bragg's plane 200), 64.73 (Bragg's plane 220) and 77.75 (Bragg's plane 311) indicating a structure of the GNPs.

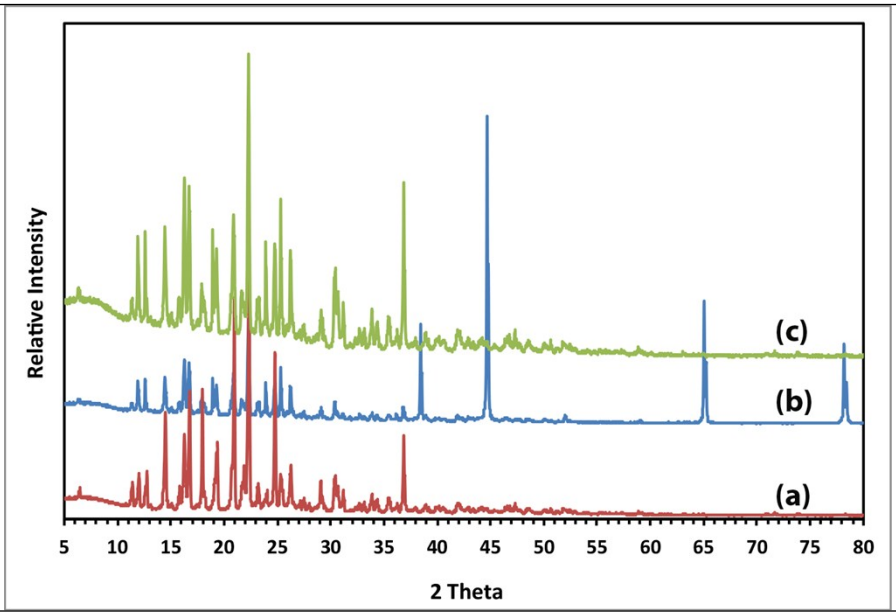

Figure 7: PXRD of solids samples of Fenofibrate, (a) Starting material purchased from Sigma-Aldrich (b) Fenofibrate crystallized from Ethyl acetate solution using functionalized gold nanoparticles and (c) Fenofibrate crystallized from Ethyl acetate solution using functionalized iron oxide nanoparticles.

Figure 8 shows the PXRD of solids samples of NaCl starting material purchased from Sigma-Aldrich and NaCl solids crystallized from water solution using functionalized gold nanoparticles.

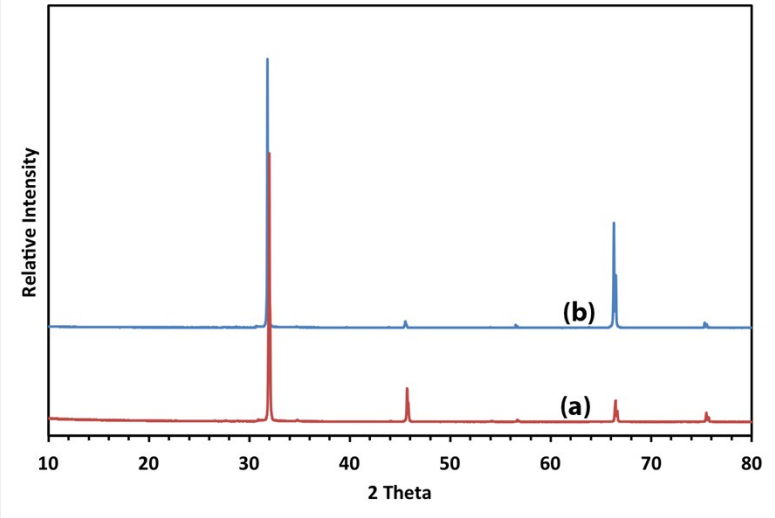

Figure 8: PXRD of solids samples of NaCl, (a) Starting material purchased from Sigma-Aldrich (b) NaCl crystallized from water solution using functionalized gold nanoparticles.

1.3 HPLC method for Fenofibrate:

Fenofibrate raw materials were obtained directly from manufacturers in China. Acetonitrile and methanol were of HPLC grade, and trifluoroacetic acid was of spectrophotometric grade obtained from Sigma Aldrich. The water used was distilled then deionized in a Barnstead Nanopure II system (Sybron/Barnstead, Boston, MA).

The liquid chromatograph consisted of an HP 1090 M HPLC with a pump, an injector, an autosampler, a variable wavelength detector (HP 1050), and a diode array detector. The column was a Symmetry ODS 3.5 mm (100×4.6 mm) (Waters, Milford, MA).

Mobile phase: The eluent consisted of acetonitrile–water–trifluoroacetic acid 700/300/1 (v/v/v) filtered through a 0.45 mm nylon filter. The flow rate was 1 ml min^{-1}.

Solutions: Fenofibrate reference standard and raw materials were dried under pumping vacuum at 60°C for 2 h prior to use. The following solutions were prepared using acetonitrile and sonicated in an ultrasonic bath, when necessary, to dissolve the compounds: (1) a standard solution of 1 mg ml−1 (accurately known) fenofibrate reference standard, and (2) a test solution of 1 mg ml−1 (accurately known) fenofibrate raw material, and a UV detector set at 280 nm.

1.4 HPLC method for 4-Nitrophenol and Benzoic acid:

An HPLC method for the determination 4-nitrophenol and Benzoic acid has been developed and validated. The method development involved the study of methanol and acetonitrile as organic modifiers, pH and flow-rate using a Chromolith RP-18e (150 mm × 4.6 mm I.D.) column. After comparing the performance the optimum analysis of these compounds was achieved using 50 mM acetate buffer (pH 5.0)-acetonitrile (80:20, v/v) as mobile phase, 1 mL min^{-1} flow-rate and UV detection at maximum absorbance wavelength of 250 nm.

1.5 HPLC results

Fenofibrate: After crystallization the sample was filtered using 0.2 µm filter and solids were analyzed using XRPD. The filtered solution was then centrifuged to separate the gold nanoparticles and the clear solution was analyzed using the HPLC to determine the change in concentration.

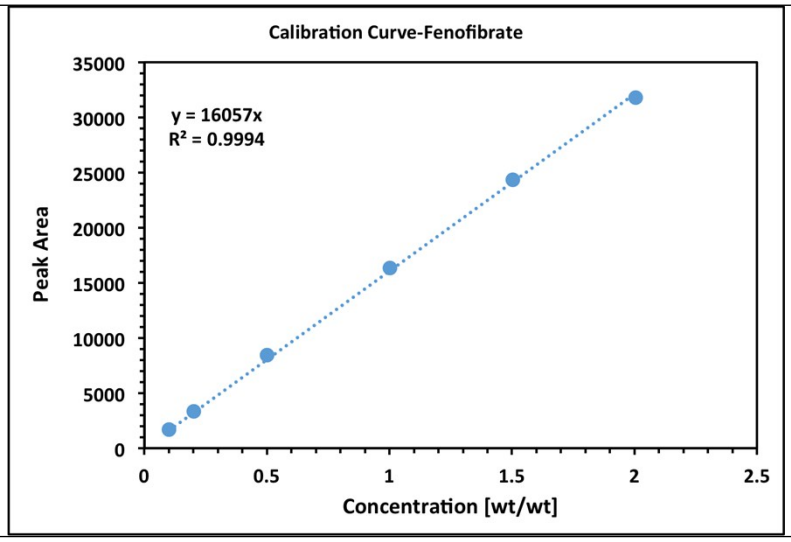

Figure 9: Calibration curve for fenofibrate as generated by measuring the peak area and absorbance at 284nm.

Sodium Chloride: The initial and final concentration of NaCl was measured using Digital Density Meter DMA4500. This instrument is used for accurate measurements of solvent density necessary for the concentration measurements. Figure 10 shows the calibration curve for NaCl as generated by measuring the density by Digital Density Meter DMA4500 at different concentration of NaCl water solutions.

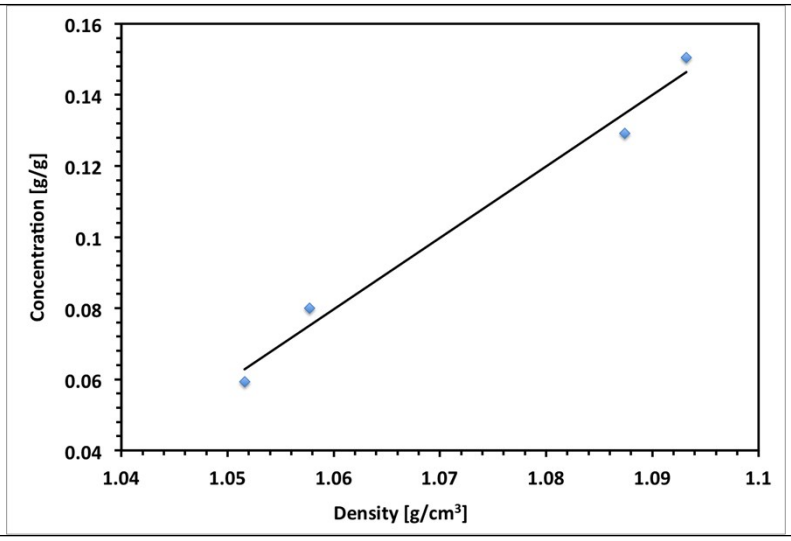

Figure 10: Calibration curve for NaCl as generated by measuring the density by Digital Density Meter DMA4500 at different concentration of NaCl water solutions.

4-Nitrophenol: After crystallization the clear solution measured by HPLC after filtration shows the concentration of 16.5 g/l, which was less then the initial concentration (20 g/l). The part of 4-nitrophenol was catalyzed to 4-Aminophenol by iron oxide as a catalyst. Figure 11 shows a calibration curve for 4-Nitrophenol as generated by measuring the peak area and absorbance at 230 nm. Figure 12 shows a schematic of conversion of 4-nitrophenol to 4-aminophenol in the presence of iron oxide as a catalyst. The HPLC results show an additional retention peaks at 2.6 and 2.7 minutes, which corresponds to 4-aminophenol (Figure 13).

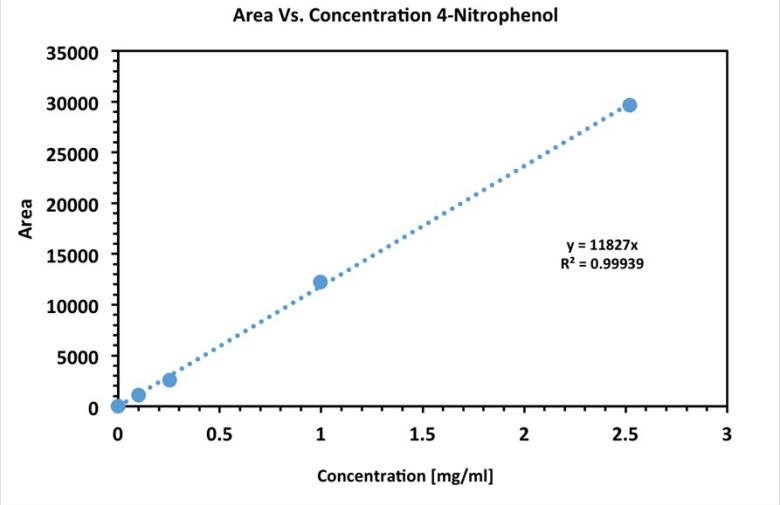

Figure 11: Calibration curve for 4-Nitrophenol as generated by measuring the peak area and absorbance at 230 nm.

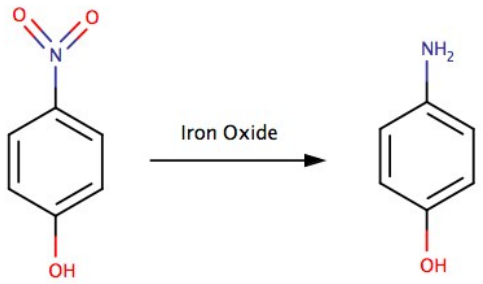

Figure 12: Schematic of conversion of 4-nitrophenol to 4-aminophenol in the presence of iron oxide as a catalyst.

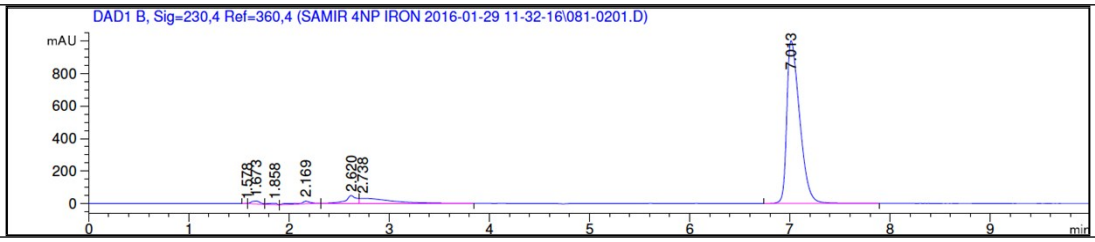

Figure 13: HPLC chromatogram for the determination of 4-nitrophenol in water at a wavelength of 230 nm. The peak at 7.013 minutes corresponds to 4-nitrophenol.

Benzoic Acid: The clear solution was analyzed using HPLC in order to determine the final concentration. Figure 14 shows the calibration curve for benzoic acid as generated by measuring the peak area and absorbance at 230 nm. The sample measured by HPLC shows the concentration of 20 g/l, which is more than 5 times higher than the equilibrium solubility of benzoic acid in water at 25 ^{o}C.

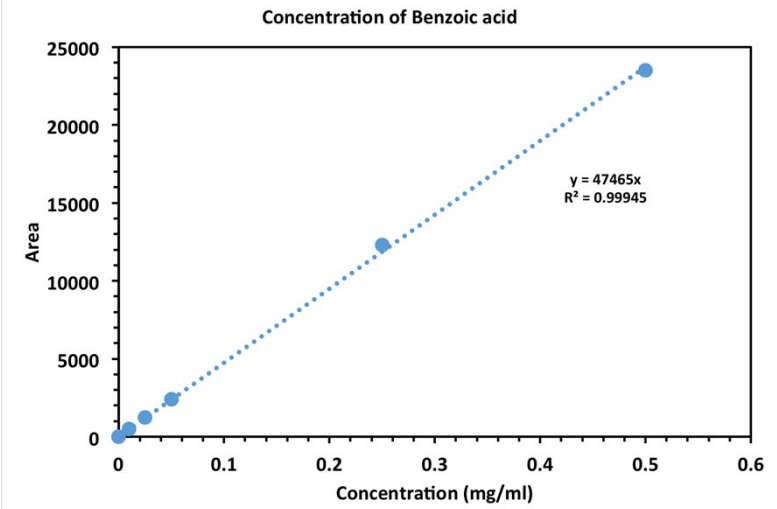

Figure 14: Calibration curve for Benzoic acid as generated by measuring the peak area and absorbance at 230 nm.

1.6 Calculations for gold and Iron oxide nanoparticles:

1. Known parameters
   Diameter of particles d (in m)
   Density of gold particles ρ_g (in Kg/m3)
   Ethanol density ρ_s (in kg/m3)
   Ethanol mol wt (kg/kmol)
   Area of each marcapto ethanol A_{thiol} (in m^2)- value from literature
   MW of gold (in kg/kmol)

2. Area of each nanoparticle = $A(Au) = 4\pi r^2$
   Mass of each particle = $Mass(Au) = (4/3\pi r^2) \times (\rho_g)$
   No of ligand on each nanoparticle = $N(ligand) = 4\pi r^2 / A_{thiol}$

3. The next step is to calculate the no of nano-particles equivalent to 1 ml of ethanol.

   1 ml of ethanol = 0.789 g
   Moles of ethanol = mass/ mol wt=0.789/46.07=0.017
   Number of molecules in 1 ml of ethanol=N_{EtOH}
   = moles * Avogadro's no.
   = 1.03E+22

   Number of nanoparticle equivalent to 1 ml of ethanol
   $Np = N_{EtOH}/N(ligand)$

   Mass of nanoparticle equivalent to 1 ml ethanol
   $M_p = N \times Mass(Au)$

Gold nanoparticles with EtOH functional group (5 nm)

Ethanol			
Diameter of particle	**D**	**5.00E-09**	M
Density of gold particles	**P**	19320	kg/m^3
Ethanol Density	ρ_{decane}	789	kg/m3
Ethanol Mol wt		46.07	kg/kmol
Area of each MercaptoEtOH	**A (from literature)[11]**	1.14E-19	m^2
MW of gold		196.96657	kg/kmol
Area of each particle	4 π r2	7.86E-17	m^2
Mass of each particle	4/3 π r3*ρ	1.27E-21	Kg
No of ligands on each particle	4 π r2/A	6.89E+02	
No of particles equivalent to 1mL	***Np***	1.50E+19	
Mass of particles eq to 1mL	***Mp***	1.89E-02	Kg
		1.89E+01	G
1mL of Ethanol		0.789	G
		0.017126112	g mol
		1.03151E+22	Molecules

Gold nanoparticles with EtOH functional group (1.8 nm)

Ethanol			
Diameter of particle	**d**	**1.80E-09**	M
Density of gold particles	**ρ**	19320	kg/m^3
Ethanol Density	ρ_{decane}	789	kg/m3
Ethanol Mol wt		46.07	kg/kmol
Area of each MercaptoEtOH	**A (from literature)[11]**	1.14E-19	m^2
MW of gold		196.96657	kg/kmol
Area of each particle	4 π r2	1.02E-17	m^2
Mass of each particle	4/3 π r3*ρ	5.90E-23	Kg
No of ligands on each particle	4 π r2/A	8.93E+01	
No of particles equivalent to 1mL	***Np***	1.15E+20	
Mass of particles eq to 1mL	***Mp***	6.82E-03	Kg
		6.82E+00	G
1mL of Ethanol		0.789	G
		0.017126112	g mol
		1.03151E+22	Molecules

Gold nanoparticles with decane functional group (5 nm)

Decane			
Diameter of particle	**D**	**5.00E-09**	M
Density of gold particles	**P**	19320	kg/m^3
Decane Density	ρ_{decane}	730	kg/m3
Decane Mol wt		142.25	kg/kmol
Area of each Mercaptodecane (A)	**A (from literature)**[12, 13]	2.14E-19	m^2
MW of gold		196.96657	kg/kmol
surface area per nanoparticle	4 π r2	7.86E-17	m^2
Mass of each particle	4/3 π r3*ρ	1.27E-21	Kg
No of ligands on each particle	4 π r2/A	3.67E+02	
No of particles equivalent to 1mL	***Np***	8.42E+18	
Mass of particles eq to 1mL	***Mp***	1.06E-02	Kg
		1.06E+01	G
1mL of decane		0.73	g
		0.00513181	g mol
		3.09089E+21	molecules

Gold nanoparticles with decane functional group (1.8 nm)

Decane			
Diameter of particle	**D**	**1.80E-09**	m
Density of gold particles	**P**	19320	kg/m^3
Decane Density	ρ_{decane}	730	kg/m3
Decane Mol wt		142.25	kg/kmol
Area of each Mercaptodecane	**A (from literature)** [12]	2.14E-19	m^2
MW of gold		196.96657	kg/kmol
Area of each particle	4 π r2	1.02E-17	m^2
Mass of each particle	4/3 π r3*ρ	5.90E-23	kg
No of ligands on each particle	4 π r2/A	4.76E+01	
No of particles equivalent to 1mL	***Np***	6.50E+19	
Mass of particles eq to 1mL	***Mp***	3.83E-03	kg
Mass of particles eq to 1mL		3.83E+00	g
1mL of decane		0.73	g
		0.00513181	g mol
		3.09089E+21	molecules

Iron oxide nanoparticles with EtOH functional group (10 nm)

Ethanol			
Diameter of particle	**d**	**1.00E-08**	m
Density of gold particles	**ρ**	865	kg/m^3
Ethanol Density	ρ_{decane}	789	kg/m3
Ethanol Mol wt		46.07	kg/kmol
Area of each glycolic acid	**A (from literature)[14]**	5.75E-19	m^2
MW of gold		159.69	kg/kmol
Area of each particle	4 π r2	3.14E-16	m^2
Mass of each particle	4/3 π r3*ρ	4.53E-22	kg
No of ligands on each particle	4 π r2/A	5.47E+02	
No of particles equivalent to 1mL	***Np***	1.89E+19	
Mass of particles eq to 1mL	***Mp***	8.55E-03	kg
		8.55E+00	g
1mL of Ethanol		0.789	g
		0.01712611	g mol
		1.0315E+22	molecules

Iron oxide nanoparticles with Decane functional group (10 nm)

Decane			
Diameter of particle	**d**	**1.00E-08**	m
Density of iron oxide nano particles	**ρ**	865	kg/m^3
Decane Density	ρ_{decane}	730	kg/m3
Decane Mol wt		142.25	kg/kmol
Area of each decanoic acid (A)	**A (from literature)[15]**	3.76E-19	m^2
MW of iron oxide		159.69	kg/kmol
surface area per nanoparticle	4 π r2	3.14E-16	m^2
Mass of each particle	4/3 π r3*ρ	4.53E-22	kg
No of ligands on each particle	4 π r2/A	8.36E+02	
No of particles equivalent to 1mL	***Np***	3.70E+18	
Mass of particles eq to 1mL	***Mp***	1.68E-03	kg
		1.68E+00	g
1mL of decane		0.73	g
		0.00513181	g mol
		3.0909E+21	molecules

1.7 Supporting references

1. S. A. Kulkarni, S. S. Kadam, H. Meekes, A. I. Stankiewicz and J. H. ter Horst, *Crystal Growth & Design*, 2013, **13**, 2435-2440.
2. S. A. Kulkarni, C. C. Weber, A. S. Myerson and J. H. ter Horst, *Langmuir*, 2014, **30**, 12368-12375.
3. A. Singh, I. S. Lee, K. Kim and A. S. Myerson, *CrystEngComm*, 2011, **13**, 24-32.
4. J. Zhang, A. Liu, Y. Han, Y. Ren, J. Gong, W. Li and J. Wang, *Crystal Growth & Design*, 2011, **11**, 5498-5506.
5. A. Z. M. Badruddoza, Z. B. Z. Shawon, W. J. D. Tay, K. Hidajat and M. S. Uddin, *Carbohydrate Polymers*, 2013, **91**, 322-332.
6. A. Z. M. Badruddoza, Z. B. Z. Shawon, M. T. Rahman, K. W. Hao, K. Hidajat and M. S. Uddin, *Chemical Engineering Journal*, 2013, **225**, 607-615.
7. D. Mishra, R. Arora, S. Lahiri, S. S. Amritphale and N. Chandra, *Protection of Metals and Physical Chemistry of Surfaces*, 2014, **50**, 628-631.
8. A. L. Andrade, D. M. Souza, M. C. Pereira, J. D. Fabris and R. Z. Domingues, *Cerâmica*, 2009, **55**, 420-424.
9. A. Atta, H. Al-Lohedan and S. Al-Hussain, *Molecules*, 2014, **19**, 11263.
10. S. K. Kumar and R. Krishnamoorti, *Annu Rev Chemi Biomol Eng*, 2010, **1**.
11. M. Bakhshpour, N. Bereli and S. Senel, *Colloids and surfaces. B, Biointerfaces*, 2014, **113**, 261-268.
12. H. G. Bagaria, E. T. Ada, M. Shamsuzzoha, D. E. Nikles and D. T. Johnson, *Langmuir*, 2006, **22**, 7732-7737.
13. G. E. Poirier, *Langmuir*, 1999, **15**, 1167-1175.
14. Wahajuddin and S. Arora, *International Journal of Nanomedicine*, 2012, **7**, 3445-3471.
15. P. Guardia, N. Pérez, A. Labarta and X. Batlle, *Langmuir*, 2010, **26**, 5843-5847.